Optica Applicata, Vol. LIII, No. 1, 2023
DOI: 10.37190/oa230110

Window layer based on ZnO and Ag thin films incorporated in solar cells as a part of hybrid energy-saving system

HADI GHOLAMZADEH[1], REZA HOSSEINI[2,*], HADI VELADI[3], HADI RAHIMI[4]

[1]Department of Electrical Engineering, Shabestar Branch, Islamic Azad University, Shabestar, Iran

[2]Department of Electrical Engineering, Khoy Branch, Islamic Azad University, khoy, Iran

[3]MSFAB, Faculty of Electrical and Computer Engineering, University of Tabriz, Tabriz, Iran

[4]Department of Physics, Shabestar Branch, Islamic Azad University, Shabestar, Iran

[*]Corresponding author: hosseini@iaukhoy.ac.ir

We have started a new research project on a hybrid power generation system consisting of piezoelectric, thermoelectric and solar cell modules. In the first step, we have focused on the antireflection coating based on zinc oxide (ZnO) and metal nanolayers incorporated in solar cells. In layered structure containing ZnO and metal nanoscale layers, we have presented the possibility of increasing wave transmission in the visible region by adding the top and bottom cap layers. The enhancement of optical transmission is very important in improving the performance of sensor protections, solar cells, UV protective films and transparent conductive display panels electrode. It is found that, the structure containing both the top and bottom cap layers (S_3) yields larger transmittance than the structures S_1 without any cap or S_2 just with one cap layer. The maximum transmittance in the visible range can be increased from 33% to 67%. In addition, for the TE mode (TM mode), the maximum value of transmission in the S_1 and S_2 structures occurs at angles close to normal incidence while in the S_3 multilayer it happens around 1 radian, that is, the behavior of the TE mode is the opposite of the TM mode. Also, when the incident angle varies, the band edges experience a blue shift. The amount of TE shift is more pronounced than TM one. Moreover, the metal with higher plasma frequency will move the band gap edges to the higher frequencies.

Keywords: solar cells, hybrid energy harvester, optical transmission, materials, photonic multilayer.

1. Introduction

Zinc oxide (ZnO) as a wide band gap II–VI semiconductor material, attracted a great attention of researchers in the last decades because of its properties, which can introduce it as a promising semiconductor oxide for a lot of applications such as thin film solar cells as a transparent conductive electrode [1,2], light-emitting diodes and lasers [3,4],

UV detectors [5], gas sensors [6,7], varistors [8], spintronic devices [9], catalysis [10], and thin film transistors [11]. ZnO is an *n*-type semiconductor material that has a transparency in the visible range ($E_g \sim 3.37$ eV), high chemical and thermal stability. The ZnO has emerged as the leading semiconductor material for photonics and optoelectronic high-frequency devices with transparency window covering ultraviolet, visible and infrared wavelengths [12,13]. It is nontoxic, abundant, inexpensive [14–16], has large exciton binding energy (~60 meV) allows efficient excitonic emission even at room temperature, thus brings promise for low-threshold and high efficiency photonic devices [17]. ZnO in the nano-scale (1–100 nm) can demonstrate the quantum confinement effects, which gives the opportunity to exhibit new physical and chemical properties. This encouraged the researchers to synthesize ZnO as a nanostructure material with various methods and in different shapes, nanoparticles, nanowires, nanorods, and nanotubes [18,19]. Moreover, ZnO can be used as a pure material in many of applications like optical and display devices or it can be doped with elements such as (Al, Ag, or Sn) to be high conductance [20] or magnetic elements (Mn, Co, or Ni) as a diluted magnetic materials [21]. ZnO coatings are used for energy-saving or heat-protecting windows. The coating lets in the visible part of the spectrum but the infrared (IR) radiation is either reflected back into the room (energy saving) or the coating does not let it into the room (heat protection), depending on which side of the window has the coating [22]. ZnO based transparent conducting oxides (TCOs) meet the stringent requirements for thin-film solar cells as it has both appropriate optoelectronic properties and high resistance to hydrogen rich plasmas [23,24]. In the field of photovoltaic applications, the main criteria that TCOs should fit are the following: first, to be highly transparent in the visible wavelength range where the solar cell is operating to minimize the photon absorption; second, to have high conductivity to reduce the resistive losses and finally, to have low carrier concentration to avoid absorption losses in the red and near-infrared (NIR) wavelength ranges. Also, the piezoelectricity in textile fibers coated in ZnO have been shown capable of fabricating "self-powered nanosystems" with everyday mechanical stress from wind or body movements [25]. ZnO films have been deposited by a number of methods like molecular beam epitaxy [26], chemical-vapor deposition [27], and pulsed laser deposition [28], radio frequency magnetron sputtering [29], spray pyrolysis [30], and thermal oxidation [31].

The possibility of creating a multilayer structure using a combination of metals and dielectric or semiconductors has opened novel possibilities for manipulating light [32–35]. Metallic thin films are candidates for various filters, waveguides, focusing and matching devices, *etc*. A transparent and electrically conductive metallic based multilayer structure in the visible range can block ultraviolet and infrared light. In this paper we purposed an improved transmittance in 1D metallic photonic crystal which is transparent to visible light. The large conductivity and negative permittivity of metals in the visible spectrum are of great interest for both linear and nonlinear devices. The enhancement of optical transmission is very important in improving the performance of sensor protections, solar cells, UV protective films and transparent conductive display panels electrodes that have applications in flat panel displays ranging

from liquid crystals to the new polymer LEDs. The supposed structure needs fewer numbers of periods to give high transmittance gap and economic cost for fabrication. Also, this kind of multilayer can be used as a polarizer for TE and TM waves. Its loss is low, and it is better than usual polarizing elements. Our supposed multilayer can be fabricated experimentally by utilizing radio frequency (RF) sputtering. Several approaches such as the plane-wave expansion (PWE) method [36], the transfer matrix method (TMM) [37], and the finite difference time domain (FDTD) method [38], the finite difference eigenvalue method [39], *etc*., have been used to calculate the photonic band structures. Here, we use the TMM one.

2. Model

Diagrams of the supposed ZnO and Ag based multilayer structures as S_1 (without cap -layers) S_2 (with top cap-layer) and S_3 (with both top and bottom cap-layers) are depicted in Fig. 1. These structures, which are embedded in air, are made of layer A and layer B materials, with thickness, electric permittivity, and magnetic permeability given by d_A and d_B, ε_A and ε_B, μ_A and μ_B, respectively.

The structures that we proposed here are formed of dielectrics (or semiconductor) and metallic inserts. The dispersive properties of a metal can be described via a complex dielectric function $\varepsilon_m(\omega) = \varepsilon_r(\omega) + i\varepsilon_i(\omega)$. Thus, the index of the metal is given by $n_m = [\varepsilon_m(\omega)]^{1/2}$, and can be modeled through $\varepsilon_m(\omega) = 1 - \omega_p^2/\omega(\omega + i\gamma)$ which is the Drude model, where ω_p is the plasma frequency and γ is the damping coefficient. Table 1 shows the plasma and damping frequencies of some metals.

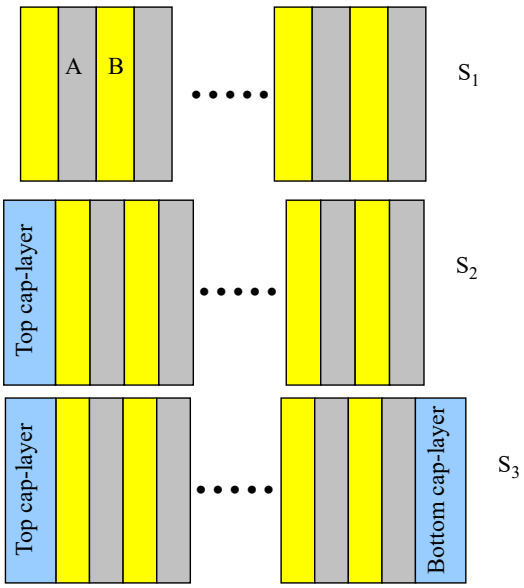

Fig. 1. Diagram of the supposed ZnO based multilayer structures as S_1 (without cap-layers) S_2 (with top cap-layer) and S_3 (with both top and bottom cap-layers).

T a b l e 1. Plasma and damping frequencies of some metals.

Metal	Plasma [PHz]	Damping [THz]	Source
Ag	2.321	5.513	BLABER *et al.* [40]
Ag	2.18	4.353	ORDAL *et al.* [41]
Ag	2.186	5.139	ZEMAN *et al.* [42]
Al	3.7	144.7	BLABER *et al.* [40]
Al	3.57	19.79	ORDAL *et al.* [41]
Al	2.911	31.12	ZEMAN and SCHATZ [42]
Cu	1.914	8.34	ORDAL *et al.* [41]
Cu	2.118	23.09	ZEMAN and SCHATZ [42]
Na	1.381	6.674	BLABER *et al.* [40]
Na	1.434	91.89	ZEMAN and SCHATZ [42]
Pt	1.244	16.73	ORDAL *et al.* [41]

T a b l e 2. Quality factors and SPP propagation lengths for some metals [44].

Wavelength regime	Metal	Q_{spp} ($\times 10^{-3}$)	L_{spp} [μm]
Ultraviolet (280 nm)	Al	0.07	2.5
Visible (650 nm)	Ag	1.2	84
	Cu	0.42	24
	Au	0.4	20
Near-Infrared (1000 nm)	Ag	2.2	340
	Cu	1.1	190
	Au	1.1	190
Telecom (1550 nm)	Ag	5	1200
	Cu	3.4	820
	Au	3.2	730

Another feature of the metallo-dielectric PCs, which we can study, is that it can be used in surface plasmon polaritons (SPP) systems. Table 2 shows the quality factors and SPP propagation lengths for four common plasmonic metals; Al, Ag, Au and Cu. It is clear that silver is the best plasmonic material in the optical, near-infrared and telecom domains (see Table 2).

Among them silver is a low-loss material, the transmission analysis of PCs made of silver yields great insight into the effects of the photonic structure on the resulting radiation. Also, silver is the metal best suited for applications in the entire visible range. It was shown that in spite of containing a total thickness of metal much greater than its skin depth at visible wavelengths, at the proper dielectric thicknesses, resonant tunneling opens up transmission windows that allow for high transmission to be achieved in regions where metals are typically opaque [45].

Here, the numerical method is based on the TMM. The TMM in electromagnetic and optics is a powerful and convenient mathematical formalism for determining the plane wave reflection and transmission characteristics of an infinitely extended slab

of a linear material. For this purpose, we assume that a wave is incident from air with angle θ onto a multilayer structure. For the transverse electric (TE) wave, the electric field E is assumed in the x direction (the dielectric layers are in the xy plane), and the z direction is normal to the interface of each layer. When such an electromagnetic wave propagates through this multilayer structure, the incident, reflected and transmitted electric fields are connected via a transfer matrix M [46] as

$$M_j(\Delta z, \omega) = \begin{bmatrix} \cos(k_z^j \Delta z) & j/q_j \sin(k_z^j \Delta z) \\ jq_j \sin(k_z^j \Delta z) & \cos(k_z^j \Delta z) \end{bmatrix} \tag{1}$$

where $k_z^j = \omega c^{-1} \sqrt{\varepsilon_j} \sqrt{\mu_j} \sqrt{1 - \sin^2(\varepsilon_j \mu_j)}$ is the component of the wave vector along the z axis, c indicates the speed of light in vacuum, $q_j = \sqrt{\varepsilon_j} / \sqrt{\mu_j} \sqrt{1 - \sin^2(\varepsilon_j \mu_j)}$ for TE polarization, and j = A, B. The transmission coefficient can be expressed as

$$t(\omega, \theta) = \frac{2\cos\theta}{(m_{11} + m_{22})\cos\theta + i(m_{12}\cos^2\theta - m_{21})} \tag{2}$$

Here $m_{ij}(i, j = 1;2)$ are the matrix elements of $X_N(\omega) = \prod_{j=1}^{N} M_j(d_j, \omega)$ which represents the total transfer matrix connecting the fields at the incidence and exit ends. The treatment for TM wave is similar to that for TE wave.

3. Results and discussion

In the visible frequency region and for both TE and TM polarizations, we study the possibility of increasing the wave transmission in the visible region by adding the top and bottom cap-layers. For this propose, three different arrangements as air/$(AB)^N$/air (S_1), air/C$(AB)^N$/air (S_2) and air/C$(AB)^N$D/air (S_3) are considered. The layers labeled as A and B, are two nano-scale building blocks. Also, C and D are considered to be top and bottom cap-layers, respectively. N is the number of period. Transmittances for the structures S_1, S_2 and S_3 are obtained by varying either the dielectric material or the metal. Here, silver (Ag) as layer A and zinc oxide (ZnO) as layer B are selected as constituent blocks. The dielectric constant of ZnO has a little dependency to frequency, so we consider it as a constant in the optical region. The ZnO is an II–VI group semiconductor with impressive optical and electrical characteristics, such as wide energy bandgap (3.37 eV), faster switching speed, higher thermal conductivity and high breakdown voltage. In this paper, we choose the structure parameters as follows: $\varepsilon_A(\omega) = 1 - \omega_p^2/\omega(\omega + i\gamma)$ with the plasma frequency $\omega_p = 2\pi \times 2.175 \times 10^{15}$ rad/s [45], the damping frequency $\gamma = 2\pi \times 4.35 \times 10^{12}$ rad/s [40], $\mu_A = 1$, $\varepsilon_B = 4.24$, $\mu_B = 1$, $d_A =$ = 50 nm, $d_B = 100$ nm and the number of periods $N = 8$. For simplicity, the material of top cap-layer (labeled C) and the material of bottom cap-layer (labeled D) are taken to be from layer A and B layers, respectively, with thicknesses $d_C = d_A/2$ and $d_D = d_B/2$.

Figure 2 shows the real part ε_r (solid line) and the imaginary part ε_i (dashed line) of Ag permittivity ε_{Ag}. The imaginary part of Ag is low and positive, also for frequen-

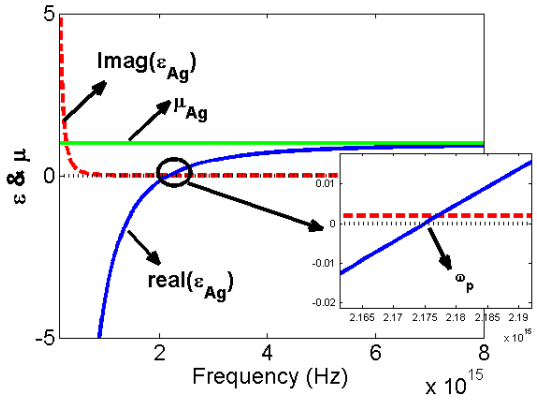

Fig. 2. The real part (solid line) and the imaginary part (dashed line) of Ag permittivity ε_{Ag} as function of frequency.

cies below ω_p the permittivity is negative. In the visible range, *i.e.*, from 0.4×10^{15} to 0.8×10^{15} Hz, the wave vector is imaginary, so Ag is opaque. Here, we focused our attention on PBG structures containing metal layers due to the low refractive index value typically offered by metals in the visible range. For the supposed S_1, S_2 and S_3 structures, the linear transmission spectra of TE (Fig. 3) and TM (Fig. 4) waves *versus*

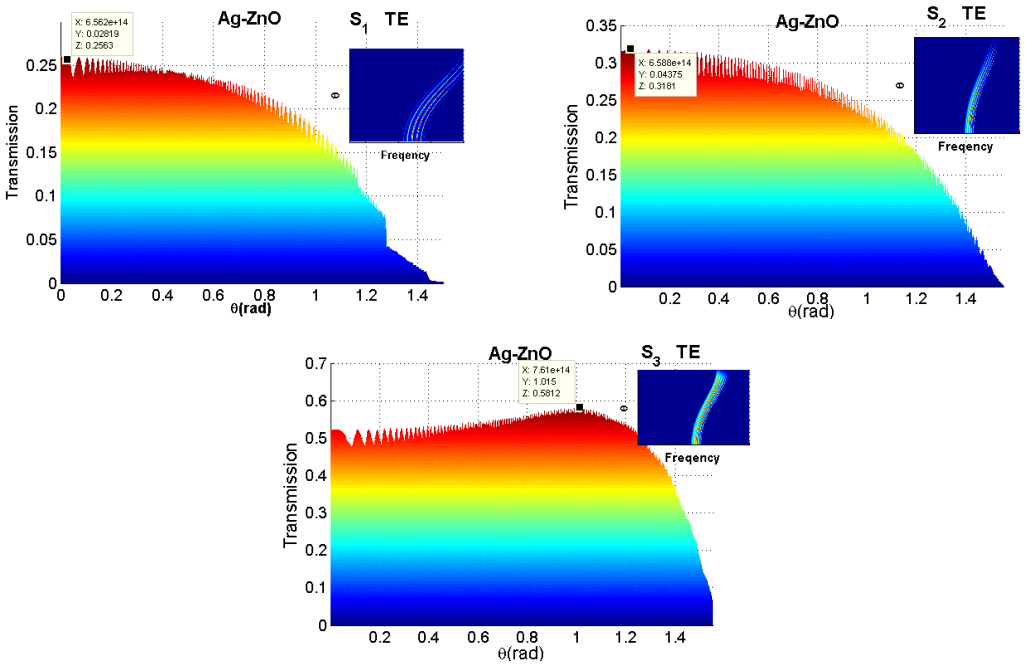

Fig. 3. The TE transmission spectra of S_1, S_2, and S_3 structures consisting of Ag and ZnO.

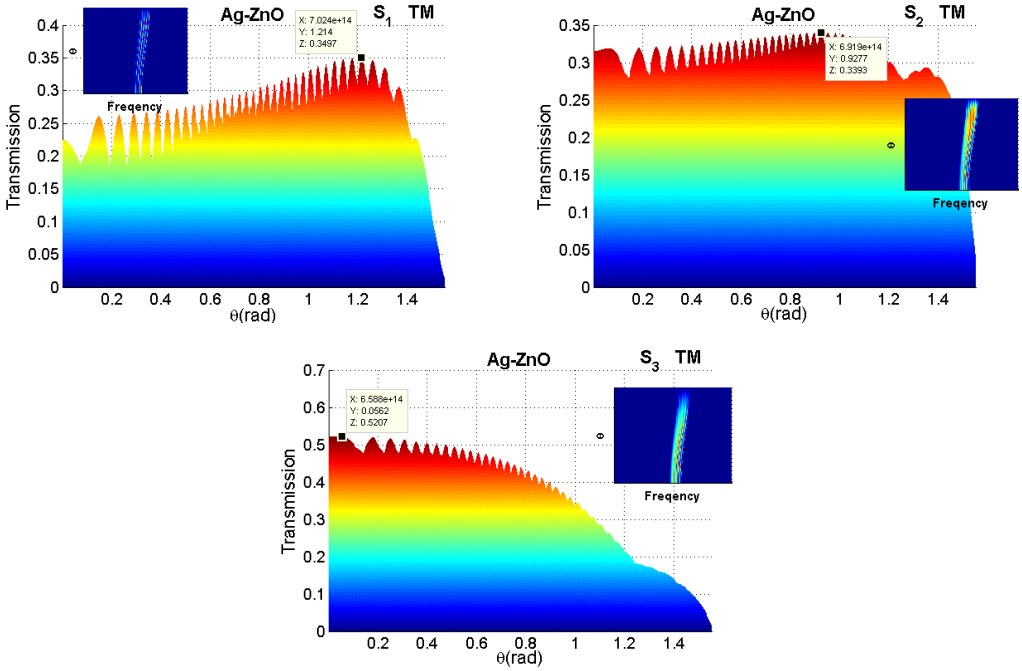

Fig. 4. The same as Fig. 3 but for TM mode.

the frequency and the incident angle are simulated in the visible range. From nearly 600 to 680 THz, one photonic band gap is observed for both polarizations which are sensitive to the incident angle, frequency, structure parameters and polarization (see Figs. 3 and 4). It is illustrated in Figs. 3 and 4 that when the incident angle varies, upper and lower band edges of Bragg gaps experience a blue shift in accordance with the Bragg–Snell law. Here, it can be proved that the phase shift of the TE waves is smaller than the phase shift of the TM waves. Therefore, for the TE mode, the amount of blue shift is more pronounced than the TM mode (see insets in figures). The influence of the incident angle on the transmission property is introduced by wave vector $k_z^j = \omega c^{-1}\sqrt{\varepsilon_j \mu_j - \sin^2\theta}$.

The dependence of transmission spectra on the incident angle is introduced by $\sin^2\theta$. If the amount of $\sin^2\theta$ exceeds the product of $\varepsilon\mu$, the wave vector will be imaginary and photonic band gap is created, consequently. In the S_1 structure $((AB)^N)$, the maximum value of TE transmission (T_{max}) is approximately 26% (see Fig. 3 for S_1). To increase the T_{max}, we offer a cap layer (labeled C) on the top of S_1 $(C(AB)^N)$ as S_2. By adding a cap layer to the top, the T_{max} is nearly enhanced to 32%. Compared to the S_1, the T_{max} is almost increased by 23%. To explore the possibility of further increase of the T_{max}, another cap-layer (labeled D) is inserted at the bottom of the S_2 as $C(AB)^ND$. The purpose of this layer is, in general, to hold the material components in place, and its exact physical properties may also vary. It is found that in the S_3 structure, the T_{max}

reach to 57% which is significant compared to the S_1 and S_2 structures. In addition, for the TE mode (the TM mode), the maximum amount of transmission in the S_1 and S_2 structures occurs at angles close to normal incidence (around 1 radian) while in the S_3 multilayer it happens around 1 radian (normal incidence), that is, the behavior of the TE mode is the opposite of the TM mode (see Figs. 3 and 4).

In Figs. 5, 6 we show the effect of different plasma frequency on the transmittance response. Because different metal has a different plasma frequency, in the structures S_1, S_2 and S_3, instead of Ag we have taken Cu metal layers with $\omega_p = 2\pi \times 1.914 \times 10^{15}$ [41]. The damping frequency of Cu is $\gamma_{Cu} = 2\pi \times 8.34 \times 10^{12}$ rad/s. For the TE and TM modes, the transmission at the top of the peaks for S_1, S_2 and S_3 structures are 24%, 31%, 50%, and 3%, 33%, 48%, respectively. As a result, regardless of the kind of the metal layer, the structure S_3 yields larger transmittance than the structures S_1 and S_2. Also, when the damping factor is involved, the T_{max} decreases, but it is not noticeable. So, the transmission peaks of selected structures are dependent on the damping factor or loss coefficient. The more damping factor, the less transmission peak. Moreover, the metal with higher plasma frequency will move the band gap to the right, namely to the higher frequencies (blue shift). In addition, our calculations for other metals, such as gold (Au) and aluminum (Al), indicate that silver is the best choice for the T_{max}. The Ag-PC has higher transmission peaks than Au-PC, due to Ag which has lower damping coefficient. The Al is very lossy and is not recommended for optical PCs. We remember that the

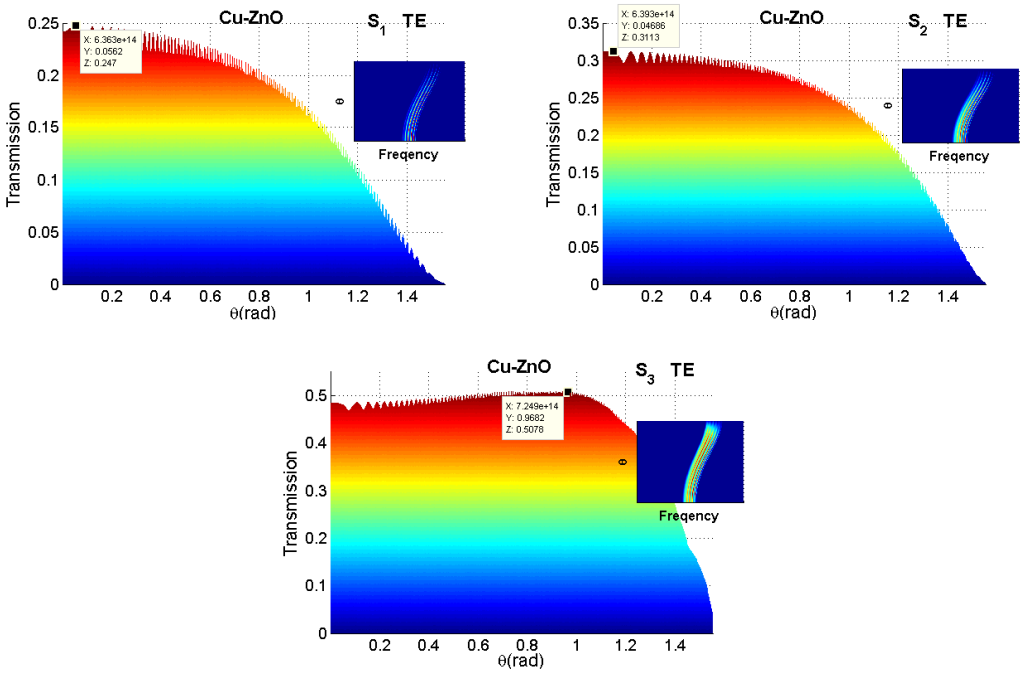

Fig. 5. The TE transmission spectra of S_1, S_2, and S_3 structures consisting of Cu and ZnO.

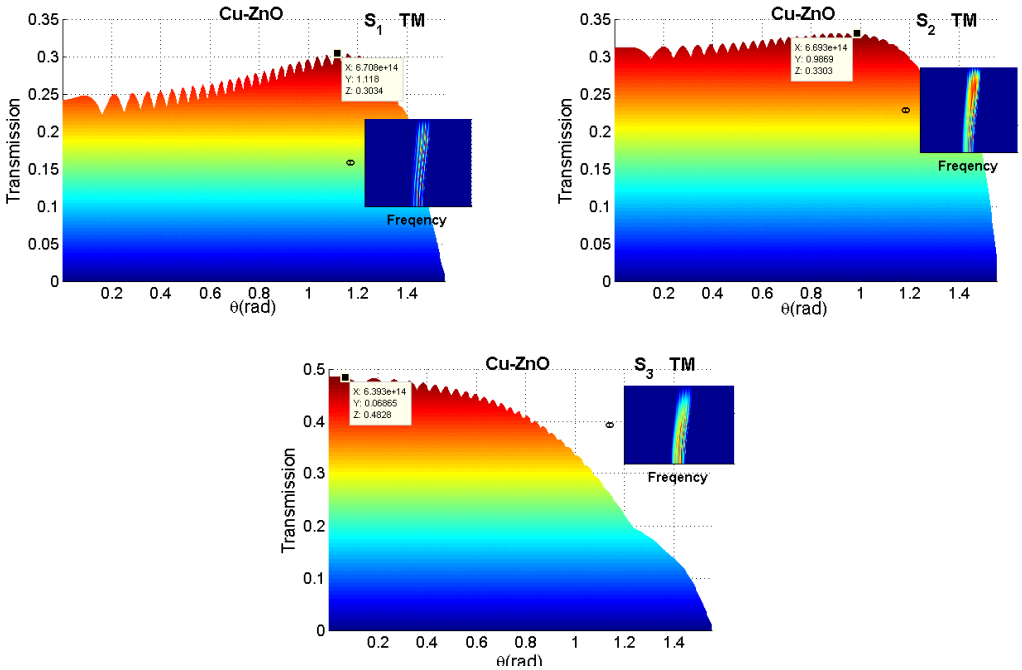

Fig. 6. The same as Fig. 5 but for TM mode.

oscillatory behavior of the transmittance spectrum, resulting from the layered structure, can be modified by varying the thickness of metals and/or dielectric layers.

4. Conclusion

In summary, in a layered structure containing metal and ZnO nano-scale layers, we have presented the possibility of increasing the wave transmission in the visible region by adding the top and bottom cap layers. It is found that, the structure S_3 (containing both the top and bottom cap layers) yields larger transmittance than the structures S_1 (without any cap layers) and S_2 (just with the top cap layer). The maximum transmittance in the visible range can be increased from 33% to 67%. In addition, for the TE mode (the TM mode), the maximum amount of transmission in the S_1 and S_2 structures occurs at angles close to normal incidence (around 1 radian) while in the S_3 multilayer it happens around 1 radian (normal incidence), that is to say, the behavior of the TE mode is the opposite of the TM mode. Also, when the incident angle varies, upper and lower band edges experience a blue shift in accordance with the Bragg–Snell law. The amount of TE shift is more pronounced than TM one, because the phase shift of the TE waves is smaller than the phase shift of the TM waves. Moreover, the metal with higher plasma frequency will move the band gap edges to the higher frequencies. The more damping factor, the less transmission.

References

[1] LIN Y.H., YANG P.C., HUANG J.S., HUANG G.D., WANG I.J., WU W.H., LIN M.Y., SU W.F., LIN C.F., *High-efficiency inverted polymer solar cells with solution-processed metal oxides*, Solar Energy Materials and Solar Cells **95**(8), 2011: 2511–2515, DOI: 10.1016/j.solmat.2011.05.005.

[2] FOO K.L., KASHIF M., HASHIM U., LIU W.W., *Effect of different solvents on the structural and optical properties of zinc oxide thin films for optoelectronic applications*, Ceramics International **40**(1), 2014: 753–761, DOI: 10.1016/j.ceramint.2013.06.065.

[3] MANDALAPU L.J., YANG Z., CHU S., LIU J.L., *Ultraviolet emission from Sb-doped p-type ZnO based heterojunction light-emitting diodes*, Applied Physics Letters **92**(12), 2008: 122101, DOI: 10.1063/1.2901018.

[4] YUEN C., YU S.F., LAU S.P., CHEN G.C.K., *Design and fabrication of ZnO light-emitting devices using filtered cathodic vacuum arc technique*, Journal of Crystal Growth **287**(1), 2006: 204–212, DOI: 10.1016/j.jcrysgro.2005.10.068.

[5] ALI M.G., SINGH S., CHAKRABARTI P., *Ultraviolet ZnO photodetectors with high gain*, Journal of Electronic Science and Technology **8**(1), 2010: 55–59, DOI: 10.3969/j.issn.1674-862X.2010.01.012.

[6] SUNIL BABU EADI, HYUN-JIN SHIN, KIM THANH NGUYEN, KI-WOO SONG, HYUN-WOONG CHOI, SEONG-HYUN KIM, HI-DOEK LEE, *Indium-gallium-zinc oxide (IGZO) thin-film gas sensors prepared via post-deposition high-pressure annealing for NO_2 detection*, Sensors and Actuators, B: Chemical **353**, 2022: 131082, DOI: 10.1016/j.snb.2021.131082.

[7] SHISHIYANU S.T., SHISHIYANU T.S., LUPAN O.I., *Sensing characteristics of tin-doped ZnO thin films as NO_2 gas sensor*, Sensors and Actuators, B: Chemical **107**(1), 2005: 379–386, DOI: 10.1016/j.snb.2004.10.030.

[8] SUVACI E., ÖZER İ.Ö., *Processing of textured zinc oxide varistors via templated grain growth*, Journal of the European Ceramic Society **25**(9), 2005: 1663–1673, DOI: 10.1016/j.jeurceramsoc.2004.05.026.

[9] MERON T., MARKOVICH G., *Ferromagnetism in colloidal Mn^{2+}-doped ZnO nanocrystals*, The Journal of Physical Chemistry B **109**(43), 2005: 20232–20236, DOI: 10.1021/jp0539775.

[10] YU H., MING H., GONG J., LI H., HUANG H., PAN K., LIU Y., KANG Z., WEI J., WANG D., *Facile synthesis of Au/ZnO nanoparticles and their enhanced photocatalytic activity for hydroxylation of benzene*, Bulletin of Materials Science **36**(3), 2013: 367–372. https://www.ias.ac.in/article/fulltext/boms/036/03/0367-0372

[11] AHN J.S., LEE K.B., *High-performance semitransparent a-$InGaZnO_4$ thin-film transistors using thin Al electrodes*, Journal of the Korean Physical Society **57**(5), 2010: 1244–1247, DOI: 10.3938/jkps.57.1244.

[12] SAMARASEKARA P., WIJESINGHE U., JAYAWEERA E.N., *Impedance and electrical properties of Cu doped ZnO thin films*, GESJ **1**(13), 2015: 512–1461.

[13] CHEBIL W., FOUZRI A., AZEZA B., SAKLY N., MGHAIETH R., LUSSON A., SALLET V., *Comparison of ZnO thin films on different substrates obtained by sol-gel process and deposited by spin-coating technique*, Indian Journal of Pure & Applied Physics **53**(8), 2015: 521–529. http://op.niscair.res.in/index.php/IJPAP/article/view/7394

[14] FOO K.L., HASHIM U., VOON C.H., KASHIF M., *Fabrication and characterization of ZnO thin films by sol-gel spin coating method for pH measurement*, Advanced Materials Research, Vol. 1109, Trans Tech Publications, Ltd., June 2015: 99–103, DOI: 10.4028/www.scientific.net/AMR.1109.99.

[15] POKHAREL J., SHRESTHA M., ZHOU L.Q., NETO V., FAN Q.H., *Oriented zinc oxide nanocrystalline thin films grown from sol–gel solution*, Journal of Coating Science and Technology **2**(2), 2015: 46–50, DOI: 10.6000/2369-3355.2015.02.02.2.

[16] SHAFURA A.K., MAMAT M.H., UZER M., SHUHAIMI A., SALMAN A., HASEEB A.K., RUSOP M., *Sensing properties of nanostructured zinc oxide-based gas sensor fabricated using immersion method*, [In] Proceedings of Malaysian International Tribology Conference, 2015: 306–307.

[17] Tang Z.K., Wong G.K.L., Yu P., Kawasaki M., Ohtomo A., Koinuma H., Segawa Y., *Room- temperature ultraviolet laser emission from self-assembled ZnO microcrystallite thin films*, Applied Physics Letters **72**(25), 1998: 3270, DOI: 10.1063/1.121620.

[18] Khanlary M.R., Vahedi V., Reyhani A., *Synthesis and characterization of ZnO nanowires by thermal oxidation of Zn thin films at various temperatures*, Molecules **17**(5), 2012: 5021–5029, DOI: 10.3390/molecules17055021.

[19] Lu H., Zhai X., Liu W., Zhang M., Guo M., *Electrodeposition of hierarchical ZnO nanorod arrays on flexible stainless steel mesh for dye-sensitized solar cell*, Thin Solid Films **586**, 2015: 46–53, DOI: 10.1016/j.tsf.2015.04.056.

[20] Kim D.H., Park J.H., Lee T.I., Myoung J.M., *Superhydrophobic Al-doped ZnO nanorods-based electrically conductive and self-cleanable antireflecting window layer for thin film solar cell*, Solar Energy Materials and Solar Cells **150**, 2016: 65–70, DOI: 10.1016/j.solmat.2016.01.041.

[21] Abdel-Galil A., Balboul M.R., Sharaf A., *Synthesis and characterization of Mn-doped ZnO diluted magnetic semiconductors*, Physica B: Condensed Matter **477**, 2008: 20–28, DOI: 10.1016/j.physb.2015.08.001.

[22] Klingshirn C., *ZnO: material, physics and applications*, ChemPhysChem **8**(6), 2007: 782–803, DOI: 10.1002/cphc.200700002.

[23] Zhao K., Xie J., Zhao Y., Han D., Wang Y., Liu B., Dong J., *Investigation on transparent, conductive ZnO:Al films deposited by atomic layer deposition process*, Nanomaterials **12**(1), 2022: 172–178, DOI: 10.3390/nano12010172.

[24] Mandal S., Singha R.K., Dhar A., Ray S.K., *Optical and structural characteristics of ZnO thin films grown by rf magnetron sputtering*, Materials Research Bulletin **43**(2), 2008: 244–250, DOI: 10.1016/j.materresbull.2007.05.006.

[25] Qin Y., Wang X., Wang Z.L., *Microfibre–nanowire hybrid structure for energy scavenging*, Nature **451**, 2008: 809–813, DOI: 10.1038/nature06601.

[26] Heo Y.W., Norton D.P., Pearton S.J., *Origin of green luminescence in ZnO thin film grown by molecular-beam epitaxy*, Journal of Applied Physics **98**(7), 2005: 73502, DOI: 10.1063/1.2064308.

[27] Tan S.T., Chen B.J., Sun X.W., Fan W.J., Kwok H.S., Zhang X.H., Chua S.J., *Blue shift of optical band gap in ZnO thin films grown by metal-organic chemical-vapor deposition*, Journal of Applied Physics **98**(1), 2005: 013505, DOI: 10.1063/1.1940137.

[28] Gadallah A.S., Nomenyo K., Couteau C., Rogers D.J., Lérondel G., *Stimulated emission from ZnO thin films with high optical gain and low loss*, Applied Physics Letters **102**(17), 2013: 171105, DOI: 10.1063/1.4803081.

[29] Wang Q.P., Zhang X.J., Wang G.Q., Chen S.H., Wu X.H., Ma H.L., *Influence of excitation light wavelength on the photoluminescence properties for ZnO films prepared by magnetron sputtering*, Applied Surface Science **254**(16), 2008: 5100–5104, DOI: 10.1016/j.apsusc.2008.02.007.

[30] Badadhe S.S., Mulla I.S., *Effect of aluminium doping on structural and gas sensing properties of zinc oxide thin films deposited by spray pyrolysis*, Sensors and Actuators, B: Chemical **156**(2), 2011: 943–948, DOI: 10.1016/j.snb.2011.03.010.

[31] Kim K.C., Kim E.K., Kim Y.S., *Growth and physical properties of sol–gel derived Co doped ZnO thin film*, Superlattices and Microstructures **42**(1–6), 2007: 246–250, DOI: 10.1016/j.spmi.2007.04.062.

[32] Minn K., Birmingham B., Ko B., Lee H.W.H., Zhang Z., *Interfacing photonic crystal fiber with a metallic nanoantenna for enhanced light nanofocusing*, Photonics Research **9**(2), 2021: 252–258, DOI: 10.1364/PRJ.411583.

[33] Palinski T.J., Hunter G.W., Tadimety A., Zhang J.X.J., *Metallic photonic crystal-based sensor for cryogenic environments*, Optics Express **27**(11), 2019: 16344–16359, DOI: 10.1364/OE.27.016344.

[34] Thapa K.B., Singh S.K., Ojha S.P., *Omnidirectional high reflector for infrared wavelength*, International Journal of Infrared and Millimeter Waves **27**(9), 2006: 1257–1268, DOI: 10.1007/s10762-006-9129-0.

[35] KESKINEN M.J., LOSCHIALPO P., FORESTER D., SCHELLENG J., *Photonic band structure and transmissivity of frequency-dependent metallic-dielectric systems*, Journal of Applied Physics **88**(10), 2000: 5785–5790, DOI: 10.1063/1.1289045.
[36] PARK J., MIN B., *Spatiotemporal plane wave expansion method for arbitrary space–time periodic photonic media*, Optics Letters **46**(3), 2021: 484–487, DOI: 10.1364/OL.411622.
[37] MISSONI L.L., ORTIZ G.P., MARTÍNEZ RICCI M.L., TORANZOS V.J., MOCHÁN L., *Rough 1D photonic crystals: A transfer matrix approach*, Optical Materials **109**, 2020: 110012, DOI: 10.1016/j.optmat.2020.110012.
[38] GAO Y., YE Q., ZHANG J., *Research on the moving plasma photonic crystals based on the novel symplectic finite-difference time-domain method*, Optik **218**, 2020: 164972, DOI: 10.1016/j.ijleo.2020.164972.
[39] SHEN L., HE S., XIAO S., *A finite-difference eigenvalue algorithm for calculating the band structure of a photonic crystal*, Computer Physics Communications **143**(3), 2002: 213–221, DOI: 10.1016/S0010-4655(01)00456-8.
[40] BLABER M.G., ARNOLD M.D., FORD M.J., *Search for the ideal plasmonic nanoshell: The effects of surface scattering and alternatives to gold and silver*, The Journal of Physical Chemistry C **113**(8), 2009: 3041–3045, DOI: 10.1021/jp810808h.
[41] ORDAL M.A., BELL R.J., ALEXANDER R.W., LONG L.L., QUERRY M.R., *Optical properties of fourteen metals in the infrared and far infrared: Al, Co, Cu, Au, Fe, Pb, Mo, Ni, Pd, Pt, Ag, Ti, V, and W*, Applied Optics **24**(24), 1985: 4493–4499, DOI: 10.1364/AO.24.004493.
[42] ZEMAN E.J., SCHATZ G.C., *An accurate electromagnetic theory study of surface enhancement factors for silver, gold, copper, lithium, sodium, aluminum, gallium, indium, zinc, and cadmium*, The Journal of Physical Chemistry **91**(3), 1987: 634–643, DOI: 10.1021/j100287a028.
[43] HOOPER I.R., SAMBLES J.R., *Dispersion of surface plasmon polaritons on short-pitch metal gratings*, Physical Review B **65**(16), 2002: 165432, DOI: 10.1103/PhysRevB.65.165432.
[44] MCPEAK K.M., JAYANTI S.V., KRESS S.J.P., MEYER S., IOTTI S., ROSSINELLI A., NORRIS D.J., *Plasmonic films can easily be better: Rules and recipes*, ACS Photonics **2**(3), 2015: 326–333, DOI: 10.1021/ph5004237.
[45] SIGALAS M.M., CHAN C.T., HO K.M., SOUKOULIS C.M., *Metallic photonic band-gap materials*, Physical Review B **52**(16), 1995: 11744–11751, DOI: 10.1103/PhysRevB.52.11744.
[46] YEH P., *Optical Waves in Layered Media*, John Wiley and Sons, New York, 1988.

Received May 29, 2022
in revised form July 21, 2022